

Effect of projectile breakup on fission-fragment mass distributions in the ${}^6,{}^7\text{Li} + {}^{238}\text{U}$ reactionsS. Santra,^{1,*} A. Pal,¹ P. K. Rath,² B. K. Nayak,¹ N. L. Singh,² D. Chattopadhyay,¹ B. R. Behera,³ Varinderjit Singh,³ A. Jhingan,⁴ P. Sugathan,⁴ K. S. Golda,⁴ S. Sodaye,⁵ S. Appannababu,² E. Prasad,⁶ and S. Kailas^{1,7}¹*Nuclear Physics Division, Bhabha Atomic Research Centre, Mumbai 400085, India*²*Department of Physics, The M. S. University of Baroda, Vadodara 390002, India*³*Department of Physics, Panjab University, Chandigarh, India*⁴*Inter University Accelerator Centre, Aruna Asaf Ali Marg, New Delhi 110067, India*⁵*Radio Chemistry Division, Bhabha Atomic Research Centre, Mumbai 400085, India*⁶*Department of Physics, Central University of Kerala, Kasaragod, Kerala 671123, India*⁷*UM-DAE Centre for Excellence in Basic Sciences, University of Mumbai, Mumbai 400 098, India*

(Received 14 October 2014; revised manuscript received 13 November 2014; published 24 December 2014)

Background: Detailed studies on the effect of the breakup of weakly bound projectile on fission are scarce. Distinguishing the events of compound nuclear (CN) fission from the breakup or transfer induced fission to understand the properties of measured fission fragments is difficult but desirable.

Purpose: To investigate the effect of projectile breakup and its breakup threshold energy on fission-fragment (FF) mass distributions and folding angle distributions for ${}^6,{}^7\text{Li} + {}^{238}\text{U}$ reactions and find out the differences in the properties of the fission events produced by complete fusion (CF) from the total fusion (TF).

Methods: The FF mass and folding angle distributions have been measured at energies around the Coulomb barrier using gas detectors by time-of-flight technique. The results are compared with the ones involving tightly bound projectiles as well as predictions from systematics to bring out the effect of the breakup.

Results: A sharp increase in the peak to valley (P:V) ratio of FF mass distribution with the decrease in bombarding energy for ${}^6,{}^7\text{Li} + {}^{238}\text{U}$ reactions is observed when all events are assumed to be CN fission. As the beam energy falls through the fusion barrier, the full width half maximum (FWHM) of the FF folding angle distribution is found to increase at sub-barrier energies, unlike the reactions involving tightly bound projectiles where a linear decrease in FWHM is expected. By selecting pure CN events from the scatter plot of the velocity components of the composite nuclei, the energy dependence of the deduced FWHM is found to be consistent with the ones involving tightly bound projectiles. Similarly, the P:V ratio obtained for the selected CN events is consistent with the theoretical calculations as well as the experimental data for the proton induced reaction forming similar CN.

Conclusions: The presence of projectile breakup induced fission and a relatively low breakup threshold for ${}^6\text{Li}$ compared to ${}^7\text{Li}$ explains the observed differences in the energy dependence of the P:V ratio and the FWHM of FF folding angle distributions for CF and TF fission in the present reactions.

DOI: [10.1103/PhysRevC.90.064620](https://doi.org/10.1103/PhysRevC.90.064620)

PACS number(s): 25.70.Jj, 25.70.Mn

I. INTRODUCTION

The shape and width of fission-fragment (FF) mass distribution provides a lot of information on the fission reaction mechanism and the structure of the compound nucleus (CN), the fragments [1] as well as the interacting nuclei [2]. For example, at low excitation energy of the CN, the FF mass distribution of actinide nuclei prefers to have a double humped shape because of the properties of fragment masses that are governed by spherical shell closure of neutrons or protons [1,3]. Similarly, a large mass width of the mass distribution and the mass-angle correlations in the mass-angle distribution of fragments are two important signatures of the quasifission process in which the composite nucleus fissions before it acquires full equilibrium in mass degrees of freedom [4,5].

The shape of the mass distribution of the fission fragments from the actinides induced by the proton or neutron is known to change with the incident energy [6,7]. At low energies, it shows a double humped distribution which changes slowly to

a single humped distribution as energy increases. However, for a reaction involving a weakly bound projectile (i.e., ${}^6\text{Li} + {}^{232}\text{Th}$), a sharp change in the shape of the mass distribution with energy was observed [8]. The ratio of the fission yield at the peak ($M \sim 137\text{--}140$) to the yield at its valley ($M \sim A/2$) is a measure of nuclear heating. The more is the value of P:V; the less is the nuclear excitation. The sharp increase in the P:V value in the fission-fragment mass distribution in the ${}^6\text{Li} + {}^{232}\text{Th}$ reaction by Itkis *et al.* [8] was concluded to be from reduced energy transfer to the composite system caused by incomplete fusion (ICF) of alpha or deuteron followed by fissions. A large probability of breakup of ${}^6\text{Li}$ into α and d made a substantial contribution to the breakup induced fission and thus the average excitation energy was much lower than the case of complete fusion (CF) followed by fission.

To investigate the above observation further, fission-fragment mass distribution measurements were made for two more reactions involving a different target (${}^{238}\text{U}$) and two weakly bound projectiles ${}^6\text{Li}$ and ${}^7\text{Li}$ with different breakup probabilities. Because ${}^7\text{Li}$ has a higher breakup threshold (hence lower breakup probability), one can expect that the P:V ratio for the ${}^7\text{Li}$ induced reaction should be smaller than

* ssantra@barc.gov.in

that of ${}^6\text{Li}$, especially at lower energies, reassuring the role of projectile breakup.

The full width half maximum (FWHM) of the folding angle distribution is another important parameter which is obtained from the measured data and provides information on possible reaction mechanisms of FF productions. The difference in the energy dependence of the FWHM of folding angles for the present reactions compared to reactions involving tightly bound projectiles would single out the effect of projectile breakup.

In the present work, we measure the FF mass and folding angle distributions for ${}^{6,7}\text{Li} + {}^{238}\text{U}$ systems at energies around the Coulomb barrier to study the effect of projectile breakup on various observables (e.g., the P:V ratio of the FF mass distributions and FWHM of FF folding angle distributions) and their dependence on the projectile breakup threshold. An attempt was made to extract the contributions from only the CF (compared to TF) in the above observables.

The paper is organized as follows. Experimental details of the measurements for the FF mass and angular distributions for ${}^{6,7}\text{Li} + {}^{238}\text{U}$ reactions are given in Sec. II. The results for fission-fragment folding angle distributions and FF mass distributions are discussed in Secs. III and IV, respectively. Finally the results are summarized in Sec. V.

II. EXPERIMENTAL DETAILS AND DATA ANALYSIS

The experiment was performed using the ${}^{6,7}\text{Li}$ beam from the 15-UD pelletron facility in Inter University Accelerator Centre, New Delhi. The ${}^{238}\text{U}$ target of thickness $\sim 100 \mu\text{g}/\text{cm}^2$ sandwiched between two layers of ${}^{12}\text{C}$ of thickness $\sim 15 \mu\text{g}/\text{cm}^2$ was used. Two multiwire proportional counter (MWPC) detectors [9] were used to detect fission fragments. These detectors are placed on two rotatable arms inside a 1.5-m diameter scattering chamber and kept on either side of the beam at a folding angle of $\theta_{\text{fold}} \sim 170^\circ$. A schematic diagram of the detector setup inside the scattering chamber is shown in Fig. 1. The MWPC1 is kept fixed on the left side of the beam with its center at $\theta = 85^\circ$ and $\phi = 90^\circ$. The center of the second detector (MWPC2) was adjusted within a very small angular range of $\theta = 84.5^\circ - 87^\circ$ depending on the beam energy, keeping its azimuthal angle ϕ fixed at 270° . The target plane was oriented at an angle of 45° with respect to the beam axis to avoid shadowing of the MWPC detectors. The distances of MWPC1 and MWPC2 from the target center are 55 cm and 40.5 cm, respectively. Each MWPC has an active area of $20 \times 10 \text{ cm}^2$ and provides position signals in horizontal (X) and vertical (Y) planes, a timing signal for time-of-flight measurements, and an energy signal equivalent to the differential energy loss in the active volume. The start of the timing was taken from a small area ($3.7 \times 3.7 \text{ cm}^2$) transmission-type fast timing multiwire proportional counter (MWPC3) which is placed on the left arm at a distance of 9.2 cm from the target center and the stop was taken from the large area MWPCs. The combination of small MWPC and any one of the large MWPCs provide absolute timing of the fission fragments. The time-of-flight signal in combination with the differential energy loss signal gives a clean separation of fission fragments from projectile and targetlike particles.

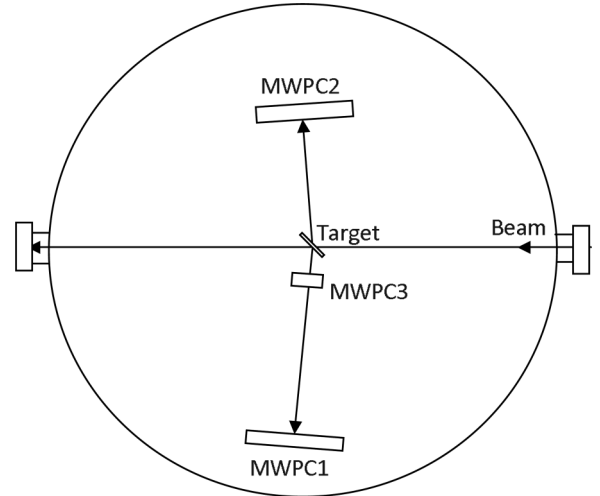


FIG. 1. A schematic diagram of the detector setup inside the scattering chamber showing the positions of three MWPC detectors with respect to the target center.

For analyzing the data of the gas detectors, the time and position signals are calibrated using standard sources. For position calibrations, a thin G-10 mask with holes of 1-mm diameter interspersed at 5 mm was put in front of each of the large MWPCs and the position signals using alpha source are acquired. For time calibration, the constant electronic delay between two detectors, which is independent of beam energy, was measured by allowing alpha particles from a source to pass through the small MWPC (MWPC3) followed by a large MWPC(1 or 2) from which start and stop of the time signal was derived, respectively. The position and time resolution of the MWPC detectors are found to be $\sim 1.3 \text{ mm}$ and $\sim 1.6 \text{ ns}$, respectively. Using the above calibration and the measured channel numbers corresponding to the position (x, y) and time-of-flight “ t ” signals for every event detected by the detector the values of scattering angle θ , azimuthal angle ϕ , and the velocity “ v ” in the laboratory frame were calculated. Assuming the CN mass m_{CN} to be equal to the sum of two FF masses “ $m_1 + m_2$ ” and applying standard kinematic transformations, different parameters in center of mass as well as the laboratory frame were calculated. Mass ratio was calculated as

$$m_R = \frac{m_2}{m_1 + m_2} = \frac{v_{1\text{c.m.}}}{v_{1\text{c.m.}} + v_{2\text{c.m.}}} \quad (1)$$

From the density plot of m_R versus “ $\theta_{\text{c.m.}}$ ” the distribution for mass ratio was found to be symmetric about $m_R = 0.5$. This ensures that the proper value of the constant electronic time delay was used in the time-of-flight calculation.

III. FOLDING ANGLE DISTRIBUTIONS

Typical fission-fragment folding angle ($\theta_{1\text{c.m.}} + \theta_{2\text{c.m.}}$) distributions (FFFAD) in the reaction plane ($\theta_{\text{c.m.}}$) versus out of the plane ($\phi_{\text{c.m.}}$) for ${}^7\text{Li}$ are shown in Fig. 2 at three energies (a) 31.4, (b) 41.4, and (c) 51.4 MeV and their respective projections on the reaction plane are given in Figs. 2(d)–2(f). It can be observed that the shape and FWHM of the FF folding

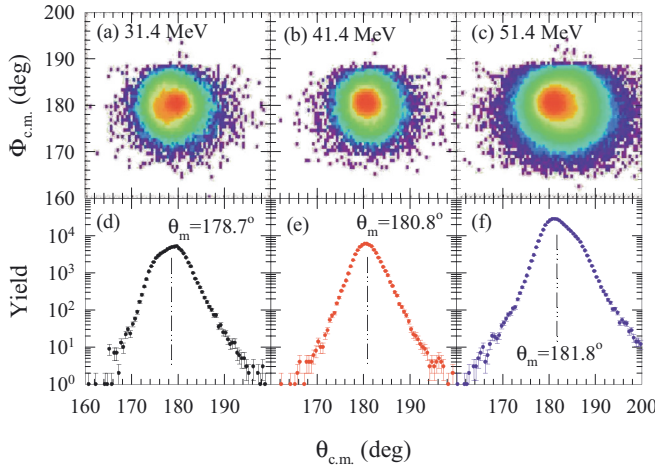


FIG. 2. (Color online) Fission-fragment folding angle distributions (FFFAD) in the reaction plane ($\theta_{c.m.}$) versus out of the plane ($\phi_{c.m.}$) for ${}^7\text{Li}$ beam energies of (a) 31.4 MeV, (b) 41.4 MeV, and (c) 51.4 MeV. Respective projections on the reaction plane are shown in (d)–(f) showing the difference in the shape, FWHM, and mean folding angle “ θ_m ” (dash-dot-dot line) of the FFFAD.

angle distributions are energy dependent. Similar observations have also been made for the second system, i.e., the ${}^6\text{Li} + {}^{238}\text{U}$ reaction. The average FF folding angle at 31.4 MeV ($< V_B$) is found to be less than 180° and at 51.4 MeV ($> V_B$) it is more than 180° , similar to the ones observed for the ${}^6\text{Li} + {}^{232}\text{Th}$ reaction [8]. This difference is understood in terms of the difference in linear momentum transfer by breakup or transfer induced fissions at different energies. At sub-barrier energies, the grazing angle is at backward angles where the breakup or transfer cross section is maximum. Here the momentum transferred to the compound nucleus (CN) by the captured d or α are higher than the complete fusion process and it makes the folding angle smaller than 180° . For above barrier energies, the grazing angle is at forward angles and hence the linear momentum transferred by a fragment to the composite nucleus is smaller than the CF process. Because part of the linear momentum is carried away by the complementary noncaptured fragment in the same direction as the beam. Hence the folding angle becomes larger than 180° . For intermediate energies, where grazing angles are around 90° , the folding angles for the CF and ICF processes are similar.

The full width at half maximum of FFFADs in ${}^{6,7}\text{Li} + {}^{238}\text{U}$ reactions was obtained at different energies and is shown in Fig. 3 as solid circles and squares, respectively. It is observed that, as one goes down in energy starting from the highest to the lowest, the FWHM of FFFAD for both the systems first decreases and then increases as the beam energy nears and falls through the fusion barrier. An increase in the FWHM with excitation energy can be understood as the spread in linear momentum of the residual CN increases with the number of evaporated neutrons. But an increase in FWHM at lower energies is something unexpected especially for reactions involving tightly bound projectiles. For example, the FWHM obtained from the experimental FF angular distribution data available for ${}^{16}\text{O} + {}^{232}\text{Th}$ [10] and ${}^{14}\text{N} + {}^{232}\text{Th}$ [11], as shown

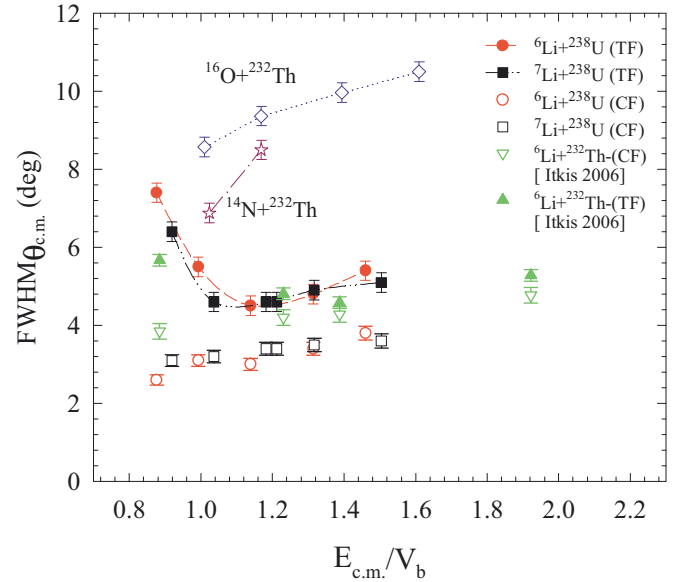


FIG. 3. (Color online) Full width at half maximum (FWHM) of FFFAD as a function of center-of-mass energy normalized to the Coulomb barrier ($E_{c.m.}/V_b$). Solid circles (squares) correspond to complete fusion events for the presently measured ${}^6\text{Li}({}^7\text{Li}) + {}^{238}\text{U}$ reaction. Literature data for the ${}^6\text{Li} + {}^{232}\text{Th}$ system (Itkis 2006 [8]) are shown as solid and hollow triangles corresponding to TF and CF events, respectively. Similarly, the data for ${}^{16}\text{O} + {}^{232}\text{Th}$ [10] and ${}^{14}\text{N} + {}^{232}\text{Th}$ [11] are represented by diamonds and stars, respectively.

in Fig. 3 as diamonds and stars, respectively, can be observed to systematically increase with the beam energy. However, the energy dependence behavior of the FWHM for the present systems is consistent with the data for the ${}^6\text{Li} + {}^{232}\text{Th}$ system with respect to total fusion (TF, solid triangles up) by Itkis *et al.* [8]. In that work, the CF and ICF contributions were separated by fitting the experimental folding angle distributions by three Gaussian peaks and the FWHM corresponding to only CF events was obtained (as shown in Fig. 3 as hollow triangles down) which shows a linear increase in FWHM with beam energy. Thus, the increase in the FWHM at lower energies is from the large contribution of ICF or breakup and transfer induced fission compared to compound nuclear fission for all the above reactions that are induced by ${}^{6,7}\text{Li}$.

To distinguish the properties of CF events from those of inclusive TF events for the present reactions, a different approach based on the velocity components of the fission fragments was adopted. For the CF, i.e., full momentum transfer events, the parallel component of the velocity (v_{\parallel}) of the fission fragments is expected to be the same as the velocity of the CN (v_{cn}) in the center of mass, and the perpendicular component of the velocity (v_{\perp}) should be zero. So, by selecting the events with the above conditions on v_{\parallel} and v_{\perp} with small tolerances one should be able to identify only the CF events and study the corresponding mass and folding angle distributions. Following the formulation given in Ref. [12], the parallel and perpendicular components of the velocity (v_{\parallel} and v_{\perp}) are

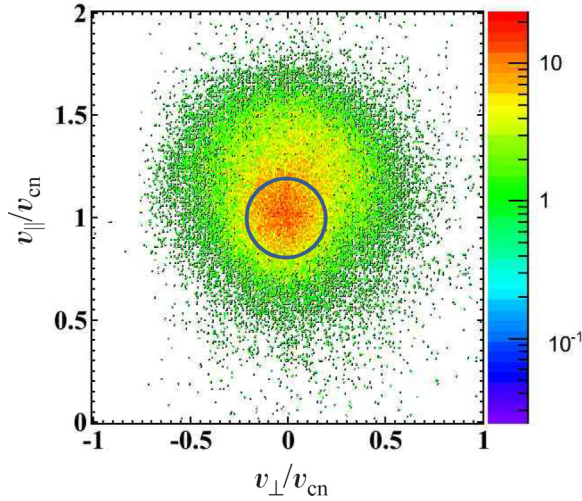


FIG. 4. (Color online) Typical scatter plot of the parallel velocity component (v_{\parallel}) versus perpendicular velocity component (v_{\perp}) of the fissioning nuclei normalized to its center-of-mass velocity (v_{cn}) for the ${}^7\text{Li} + {}^{238}\text{U}$ reaction at $E_{\text{lab}} = 31.4$ MeV. A circular cut with radius $[(v_{\parallel} - 1)^2 + v_{\perp}^2]^{1/2} \leq 0.2v_{\text{cn}}$ corresponds to pure CF events.

calculated as

$$v_{\parallel} = \frac{u_1 w_2 + u_2 w_1}{u_1 + u_2}, \quad (2)$$

$$v_{\perp} = \frac{u_1 u_2 \sin \phi_{12}}{\sqrt{u_1^2 + u_2^2 - 2u_1 u_2 \cos \phi_{12}}}. \quad (3)$$

Here, $u_i = v_i \sin \theta_i$ and $w_i = v_i \cos \theta_i$ with v_i and θ_i being the laboratory velocity and polar angle of one ($i = 1$ or 2) of the fission fragments respectively. The azimuthal folding angle in the laboratory is given as ϕ_{12} . Figure 4 shows the plot of the above velocity components normalized to the center-of-mass velocity of the CN, i.e., $v_{\parallel}/v_{\text{cn}}$ versus v_{\perp}/v_{cn} . Although there are several measurements involving heavier projectiles where one can differentiate the CN fissions from transfer induced fissions using such velocity plots, it was not possible for the present reactions to make a clear distinction between ICF and CF events. This may be because of a very small difference in mass units of the projectile and breakup fragments compared to the fission fragments leading to a negligible change in their velocity components. So, from the above exercise it is difficult to disentangle the contribution of CF and ICF completely. However, the intense peak at the center around coordinate (0,1) must correspond to the CF events.

By selecting a small circular region with a radius of $[(v_{\parallel} - 1)^2 + v_{\perp}^2]^{1/2} \leq 0.2v_{\text{cn}}$ the present data have been re-analyzed to obtain the properties of CF events only and compare with those for TF events. A tighter cut with an even smaller tolerance ($<0.2v_{\text{cn}}$) could also be used to enhance the purity of the CF events but at the expense of good statistics. The results for the FWHM of the FF folding angle distributions corresponding to the selected CF events for the ${}^6\text{Li}({}^7\text{Li}) + {}^{238}\text{U}$ reaction are shown as open circles (squares) in Fig. 3. These values are much smaller compared to the TF events (solid circles and squares) and show a systematic

increase in FWHM as energy increases from below barrier to above barrier energies.

IV. MASS DISTRIBUTION

In the present measurements, the events for breakup or transfer induced fissions could not be separated completely from the CN fissions. So, first the data were analyzed assuming all the events are from CN fission. Later, only the central events with $v_{\parallel} \sim v_{\text{cn}}$ and $v_{\perp} \sim 0$, supposed to be pure CN events, are analyzed and compared with the inclusive events to find the difference. Results for mass distribution assuming all to be CN fission are given in Fig. 5. It shows the yield of fission fragments of different masses detected in the ${}^6\text{Li} + {}^{238}\text{U}$ reaction (upper panel) at beam energies of 30, 34, 39, 45, and 50 MeV and in the ${}^7\text{Li} + {}^{238}\text{U}$ reaction (lower panel) at beam energies of 31.4, 35.4, 40.4, 41.4, 45, and 51.4 MeV. The double humped structure in the mass distribution is found to be most prominent at the lowest energy for both the reactions, as expected. As the beam energy increases, the two humps gradually come closer to become a single hump with symmetric mass distribution.

The ratio of the peak to valley of the above fission-fragment mass distributions are obtained for ${}^{6,7}\text{Li} + {}^{238}\text{U}$ reactions

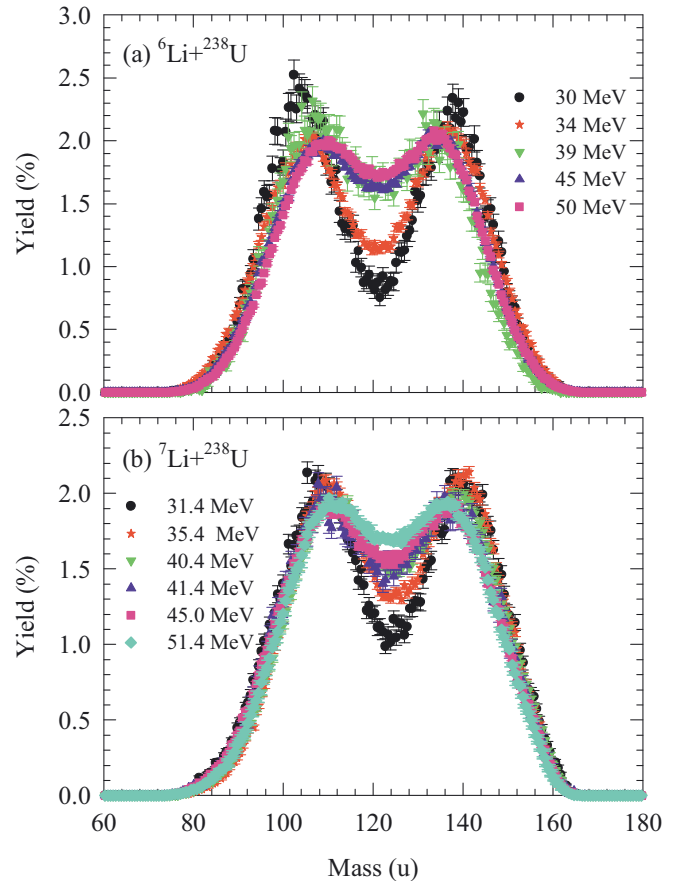


FIG. 5. (Color online) Yield of fission fragments as a function of fragment mass obtained from (a) ${}^6\text{Li} + {}^{238}\text{U}$ reaction (upper panel) and (b) ${}^7\text{Li} + {}^{238}\text{U}$ reaction (lower panel) at several beam energies, showing the change in the shape of mass distribution with energy.

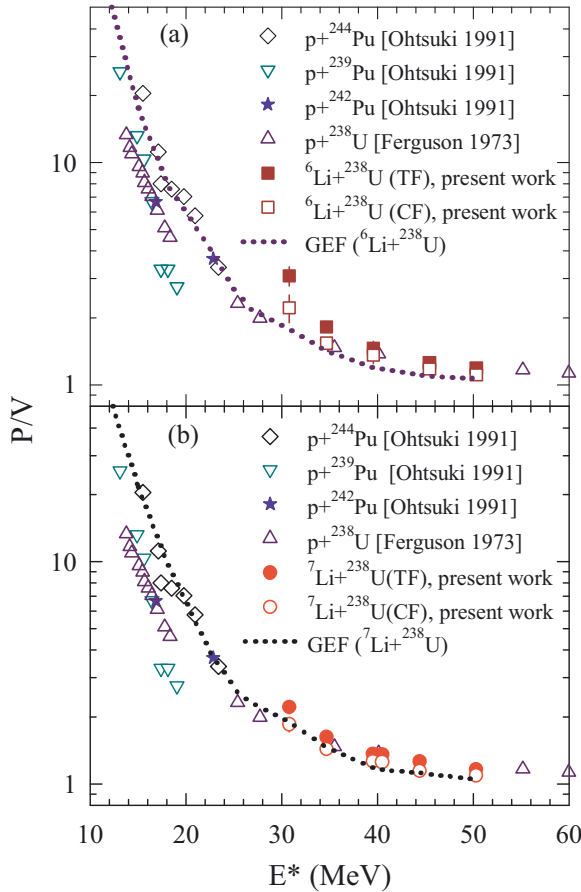


FIG. 6. (Color online) Ratio of peak to valley (P:V) of the measured fission-fragment mass distribution for (a) ${}^6\text{Li} + {}^{238}\text{U}$ and (b) ${}^7\text{Li} + {}^{238}\text{U}$ are shown as solid squares (upper panel) and solid circles (lower panel), respectively. Corresponding P:V ratio derived only for CF events are shown as open squares and open circles, respectively. Literature data for $p + {}^{239,242,244}\text{Pu}$ (Ohtsuki 1991 [13]) and $p + {}^{238}\text{U}$ (Ferguson 1973 [7]) along with results of the GEF code (dotted line) are also compared. See text for details.

at different energies and plotted in Fig. 6 as solid squares (upper panel) and solid circles (lower panel), respectively. The P/V values obtained from the literature [7,13] for proton induced reactions forming similar compound nuclei, e.g., for ${}^{244}\text{Pu}(p, f)$ (diamonds), ${}^{242}\text{Pu}(p, f)$ (stars), ${}^{239}\text{Pu}(p, f)$ (triangles down), and ${}^{238}\text{U}(p, f)$ (triangles up) fission reactions along with the theoretical results obtained from the GEF code, version 2014/2.1 [14] (dotted line), are also shown in the above figure to compare the present results. The theoretical results for P:V values are found to be consistent with the literature data for the $p + {}^{244}\text{Pu}$ reaction (that forms the same CN as in the ${}^7\text{Li} + {}^{238}\text{U}$ reaction) and they are slightly higher than $p + {}^{239,242}\text{U}$ systems at the available excitation energy range. It is interesting to observe that the peak to valley ratio for ${}^6\text{Li} + {}^{238}\text{U}$ (solid squares) and ${}^7\text{Li} + {}^{238}\text{U}$ (solid circles) are systematically higher than the GEF predictions (dotted line) over the measured excitation energy range. The increase in the P:V ratio for ${}^6\text{Li} + {}^{238}\text{U}$ is sharper than

that of ${}^7\text{Li} + {}^{238}\text{U}$. In case of ${}^6\text{Li} + {}^{238}\text{U}$, the P:V ratio measured at the lowest excitation energy ($E_x = 30.8$ MeV assuming CF) can be obtained from the GEF prediction at much lower excitation energy ($E_x \approx 24.2$ MeV). This implies that the average excitation energy of the compound nuclei formed in the above reactions must be smaller, because of the contributions of ICF, than the one we have calculated assuming CF only. However, for ${}^7\text{Li} + {}^{238}\text{U}$, the difference between the measured P:V ratio and the prediction is smaller. It implies that the ICF contribution is smaller for the latter system compared to the case of ${}^6\text{Li} + {}^{238}\text{U}$. This observation is consistent with the fission cross-section data of Ref. [15] as well as Ref. [16] where it was observed that the fission cross sections at sub-barrier energies for ${}^6\text{Li} + {}^{232}\text{Th}, {}^{235,238}\text{U}$ are much larger than ${}^7\text{Li} + {}^{232}\text{Th}, {}^{235,238}\text{U}$.

The P:V ratio of the mass distributions obtained above contains the contribution of both CF and ICF. To isolate the properties associated with CF from TF, next we analyze only the events lying inside the circle of radius $[(v_{\parallel} - 1)^2 + v_{\perp}^2]^{1/2} \leq 0.2v_{\text{cn}}$ in Fig. 4. The P:V ratio, thus obtained, are shown as open squares (upper panel) and open circles (lower panel) in Fig. 6 for ${}^6\text{Li} + {}^{238}\text{U}$ and ${}^7\text{Li} + {}^{238}\text{U}$ reactions, respectively. Interestingly these values are very close to the theoretical predictions made by GEF. So, the additional contributions towards P:V values obtained earlier are certainly due to the ICF channels. If the P:V ratios of individual ICF channels (e.g., $\alpha + {}^{238}\text{U}$, $d + {}^{238}\text{U}$, etc.) and their contributions towards the total fusion of the present systems are known then one can calculate the effective excitation energy of the composite nuclei formed at a particular beam energy.

To investigate further the effect of projectile breakup on FF folding angles and mass distribution, the events corresponding to different folding angles are selected and the P:V values of the corresponding mass distributions are derived. As mentioned earlier, at low bombarding energies, the events with folding angles less than 180° in center of mass, as observed in Fig. 2(a), correspond to the fissions induced by projectile breakup fragments. To demonstrate this, the fission events only with folding angles less than 175° are selected and their mass distributions for ${}^{6,7}\text{Li} + {}^{238}\text{U}$ are obtained and are shown in Fig. 7(a) as open and solid circles, respectively. Similarly, the fission events with folding angles $179^\circ \leq \theta \leq 181^\circ$ corresponding to complete fusion are selected and their mass distributions are shown in Fig. 7(b). It can be observed that the P:V ratios for the mass distributions in Fig. 7(a) are much larger than the ones in Fig. 7(b) implying that the excitation energy of the compound nucleus corresponding to the former must be much lower than the latter. And, this reduction in CN excitation energy must be due to incomplete fusion of the projectile with the target. Similar results have also been obtained at the highest bombarding energy with $E_x = 50.3$ MeV as shown in Figs. 7(c) and 7(d). Here, the fission events with folding angles more than 185° have been chosen to represent the incomplete fusion.

The folding angle dependence of P:V ratio of the FF mass distributions in the ${}^{6,7}\text{Li} + {}^{238}\text{U}$ reaction over a large range and in small steps of folding angle is shown in Fig. 8.

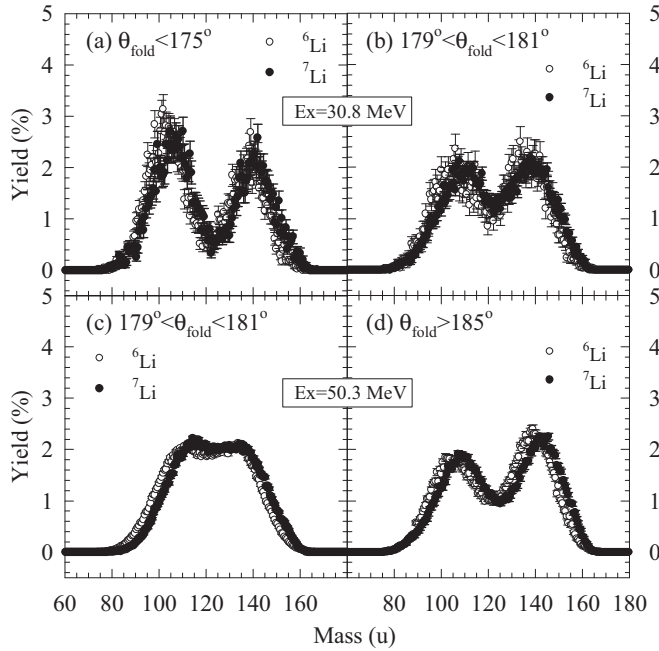


FIG. 7. Fission-fragment mass distribution for the ${}^{6,7}\text{Li} + {}^{238}\text{U}$ reaction, with CN excitation energy $E_x = 30.8$ MeV, for the fission events corresponding to folding angles (a) less than 175° and (b) $179^\circ \leq \theta_{\text{fold}} \leq 181^\circ$. At $E_x = 50.3$ MeV, the mass distributions are for the fission events with folding angles (c) $179^\circ \leq \theta_{\text{fold}} \leq 181^\circ$ and (d) more than 185° .

Here, the P:V ratio of the mass distributions of the events corresponding to small folding angle bins ($\Delta\theta_{\text{fold}} \sim 2.5^\circ$ or more), are obtained for two (measured minimum and maximum) excitation energies: (a) 30.8 MeV and (b) 50.3 MeV. For lower CN excitation energy, the P:V ratio is found to increase with the decrease of θ_{fold} below 180° . And, for higher CN excitation energy the effect is reversed, where the P:V ratio increases with the increase of θ_{fold} above 180° . The above figure shows the region of folding angles over which

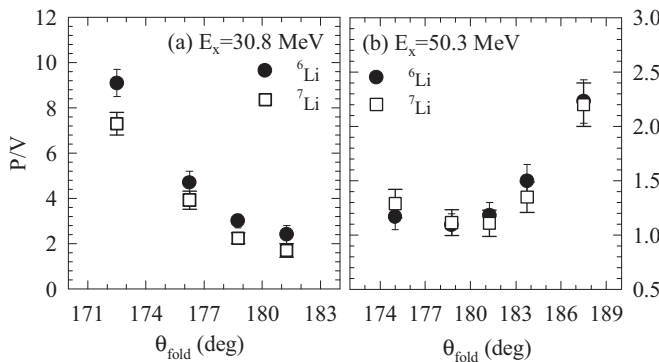


FIG. 8. P:V ratio of the fission-fragment mass distribution for the ${}^{6,7}\text{Li} + {}^{238}\text{U}$ reaction as a function of FF folding angle “ θ_{fold} ” in steps of $\Delta\theta_{\text{fold}} \sim 2.5^\circ$ or more, at two excitation energies: (a) 30.8 MeV and (b) 50.3 MeV.

the CF and ICF dominate for both the reactions at two extreme excitation energies.

V. SUMMARY

Fission-fragment mass and folding angle distributions for ${}^{6,7}\text{Li} + {}^{238}\text{U}$ reactions are measured at energies close to and above the Coulomb barrier. First, the data were analyzed assuming all fission events are via CN. The energy dependence of the FWHM of FF folding angle distributions for the present systems shows different behavior compared to the one for reactions involving tightly bound projectiles (e.g., ${}^{14}\text{N}, {}^{16}\text{O} + {}^{232}\text{Th}$). The FWHM for the present systems first decreases and then starts increasing as the beam energy increases past the Coulomb barrier, unlike the latter systems where it increases monotonically with energy from the sub-barrier to above barrier region. Behavior of the present systems is consistent with that of the ${}^6\text{Li} + {}^{232}\text{Th}$ system for which it is established that the increase in FWHM is mainly from additional contribution of breakup induced fission.

The energy dependence of the peak to valley (P:V) ratio of the mass distributions for the two reactions was also found to be different. The values of the P:V ratio are found to be higher compared to the proton induced reactions with actinide targets forming similar compound nuclei as well as the predictions from a systematics at the same excitation energies. A sharp increase in the P:V ratio as energy decreases below the Coulomb barrier indicates the population of composite nuclei with relatively less excitation energy than expected. This is possible when there is a significant contribution of breakup or transfer induced fission where the fragments transferred to the composite nuclei carried less excitation energy. The folding angle dependence of the P:V ratio of the mass distribution was obtained at two different excitation energies of the composite system. It differentiates the region of dominance of CF and ICF on folding angles. It also confirms that the large P:V values are mainly contributed by incomplete fusion in which the folding angle is less (more) than 180° in center of mass for bombarding energies less (more) than the Coulomb barrier of target+projectile.

By putting a gate on the scatter plot of the velocity components of the composite nuclei, with $v_{\parallel} \sim v_{\text{cn}}$ and $v_{\perp} \sim 0$, the above values for pure CF events are derived. The energy dependence of the FWHM of the folding angle distributions and the P/V ratio of the mass distributions for CF events are found to be different from the TF events but similar to the ones for reactions involving tightly bound projectiles as well as the predictions from the systematics.

ACKNOWLEDGMENTS

The authors would like to thank the pelletron crew of IUAC for the smooth operation of the accelerator during the experiments. One of the authors (S.K.) would like to acknowledge D.A.E. for the support through the Raja Ramanna Fellowship. Thanks are also due to D. Patel for her help during the experiment.

- [1] D. M. Gorodisskiy, S. Mulgin, V. Okolovich, A. Rusanov, and S. Zhdanov, *Phys. Lett. B* **548**, 45 (2002).
- [2] C. Simenel, D. J. Hinde, R. du Rietz, M. Dasgupta, M. Evers, C. J. Lin, D. H. Luong, and A. Wakhle, *Phys. Lett. B* **710**, 607 (2012).
- [3] B. D. Wilkins, E. P. Steinberg, and R. R. Chasman, *Phys. Rev. C* **14**, 1832 (1976).
- [4] J. Toke, R. Bock, G. Dai, A. Gobbi, S. Gralla, K. Hildenbrand, J. Kuzminski, W. Müller, A. Olmi, H. Stelzer *et al.*, *Nucl. Phys. A* **440**, 327 (1985).
- [5] W. Q. Shen, J. Albinski, A. Gobbi, S. Gralla, K. D. Hildenbrand, N. Herrmann, J. Kuzminski, W. F. J. Muller, H. Stelzer, J. Tke *et al.*, *Phys. Rev. C* **36**, 115 (1987).
- [6] G. N. Kniajeva, L. Krupa, A. Bogachev, G. Chubarian, O. Dorvaux, I. Itkis, M. Itkis, J. Kliman, S. Khlebnikov, N. Kondratiev *et al.*, *Nucl. Phys. A* **734**, E25 (2004).
- [7] R. L. Ferguson, F. Plasil, F. Pleasonton, S. C. Burnett, and H. W. Schmitt, *Phys. Rev. C* **7**, 2510 (1973).
- [8] I. M. Itkis, A. A. Bogachev, A. Y. Chizhov, D. M. Gorodisskiy, M. G. Itkis, G. N. Knyazheva, N. A. Kondratiev, E. M. Kozulin, L. Krupa, S. I. Mulgin *et al.*, *Phys. Lett. B* **640**, 23 (2006).
- [9] A. Jhingan, P. Sugathan, K. S. Golda, R. P. Singh, T. Varughese, H. Singh, B. R. Behera, and S. K. Mandal, *Rev. Sci. Instrum.* **80**, 123502 (2009).
- [10] R. K. Choudhury, A. Saxena, A. Chatterjee, D. V. Shetty, S. S. Kapoor, M. Cinausero, L. Corradi, E. Farnea, E. Fioretto, A. Gadea *et al.*, *Phys. Rev. C* **60**, 054609 (1999).
- [11] B. R. Behera, M. Satpathy, S. Jena, S. Kailas, R. G. Thomas, K. Mahata, A. Chatterjee, S. Roy, P. Basu, M. K. Sharan *et al.*, *Phys. Rev. C* **69**, 064603 (2004).
- [12] D. J. Hinde, M. Dasgupta, J. R. Leigh, J. C. Mein, C. R. Morton, J. O. Newton, and H. Timmers, *Phys. Rev. C* **53**, 1290 (1996).
- [13] T. Ohtsuki, Y. Nagame, K. Tsukada, N. Shinohara, S. Baba, K. Hashimoto, I. Nishinaka, K. Sueki, Y. Hatsukawa, K. Hata *et al.*, *Phys. Rev. C* **44**, 1405 (1991).
- [14] B. Jurado and K. H. Schmidt <http://www.khs-erzhausen.de/GEF-2014-2-1.html> Computer code GEF code, Version 2.1, 2014.
- [15] H. Freiesleben, G. T. Rizzo, and J. R. Huizenga, *Phys. Rev. C* **12**, 42 (1975).
- [16] A. Parihari, S. Santra, A. Pal, N. L. Singh, K. Mahata, B. K. Nayak, R. Tripathi, K. Ramachandran, P. K. Rath, R. Chakrabarti *et al.*, *Phys. Rev. C* **90**, 014603 (2014).